GEOPHYSICS, VOL. 74, NO. 6 (NOVEMBER-DECEMBER 2009); P. B209–B219, 12 FIGS., 2 TABLES.
10.1190/1.3230495

Case History

3D seismic reflection imaging of volcanic-hosted massive sulfide deposits: Insights from reprocessing Halfmile Lake data, New Brunswick, Canada

Alireza Malehmir[1] and Gilles Bellefleur[2]

ABSTRACT

Three-dimensional seismic reflection data from the Halfmile Lake area, New Brunswick, Canada, was reprocessed over an 18-km^2 grid to improve the seismic signatures of a 5-million-ton volcanic-hosted massive sulfide (VHMS) deposit located at 1200-m depth, known as the deep zone, as well as key host-rock structures. We chose a prestack dip moveout (DMO) and poststack migration processing sequence to preserve the possible diffraction signature of the deep VHMS zone. Despite the high level of source-generated noise and large statics caused by near-surface conditions, our processing results revealed improved 3D seismic images for shallow and deep structures. Many of the imaged structures were easily correlated with known lithological contacts constrained by boreholes and petrophysical measurements. A short, flat-lying segment of high-amplitude reflection at about 800-m depth in the unmigrated cube was interpreted to originate from a small portion of the lower VHMS zone. The DMO stack was characterized by a large, high-amplitude asymmetric diffraction signature originating from the deep VHMS zone. The asymmetry of the diffraction hyperbola relative to the location of the deep zone was interpreted as resulting from a shape effect from the zone, with the strongest amplitudes along the diffraction hyperbola found north-northwest of the apex. This indicated that the deep VHMS zone dips in a similar direction. This diagnostic diffraction signature was not preserved with the prestack migration approach previously implemented for processing Halfmile Lake data.

INTRODUCTION

Geophysical exploration of volcanic-hosted massive sulfide (VHMS) deposits traditionally has relied on nonseismic methods such as electromagnetic and potential field techniques. However, the increasing ambiguity of nonseismic interpretation methods with depth makes seismic reflection methods favorable for targeting deep-seated (>1000 m) VHMS deposits (Eaton et al., 2003). Following petrophysical measurements of P- and S-wave velocities and densities of host rocks and mineralized zones (Salisbury et al., 2000), it became evident that VHMS deposits in a typical volcano-sedimentary setting could generate high acoustic-impedance values.

Early 2D and 3D seismic reflection studies over known VHMS deposits in Canada also provided encouraging results and indications of a seismic response from orebodies (Milkereit et al., 1996; Adam et al., 2000), often revealing complex seismic images open to varied interpretations. Today, there are several published accounts of 2D and 3D seismic reflection studies designed to directly target mineral deposits (Pretorius et al., 1989; Milkereit et al., 1996; Adam et al., 2000; Milkereit et al., 2000; Adam et al., 2003; Pretorius et al., 2003; Stevenson et al., 2003) or guide exploration programs by imaging key geologic structures associated with mineral deposits (Verpaelst et al., 1995; Wu et al., 1995; Adam et al., 1996; Drummond et al., 1997; Roberts et al., 2003; Malehmir et al., 2006; Tryggvason et al., 2006).

Manuscript received by the Editor 5 January 2009; revised manuscript received 22 April 2009; published online 4 December 2009.
[1]Formerly Geological Survey of Canada, Ottawa, Ontario, Canada; presently Uppsala University, Department of Earth Sciences, Uppsala, Sweden. E-mail: alireza.malehmir@geo.uu.se.
[2]Geological Survey of Canada, Ottawa, Ontario, Canada. E-mail: gbellefl@nrcan-rncan.gc.ca.

In 1998, Noranda Inc. acquired a 3D seismic-reflection data set covering an area of approximately 18 km^2 over the Halfmile Lake deposit located in the Bathurst mining camp of New Brunswick, Canada (Figure 1). The aim of the survey was to investigate the application of seismic reflection data for targeting deep-seated VHMS deposits. The 3D prestack migration data processing conducted by Noranda Inc. identified several high-amplitude seismic anomalies that subsequently were drilled. Drilling one of the targeted anomalies resulted in discovering approximately 5 million tons of VHMS mineralization at a depth of 1200 m.

The mineralization zone, now known as the deep zone (Figure 2), is a massive pyrite-rich body approximately 300 m long, 100 m wide downdip, and 50 m thick (Matthews, 2002). The deep zone mainly dips to the north at about 50° to 60° with an overall east-west orientation. The total inferred assay for the deep zone obtained from several boreholes is 0.15% copper, 1.60% lead, 6.86% zinc, and 17 g/t silver (S. Taylor, personal communication, 2008). The deep zone is subeconomic and requires additional reserves (in the immediate vicinity) to make it of economic interest. Key results from the seismic work were published (Matthews, 2002), but detailed information on the processing flow and interpretation that led to other drilling targets is not available publicly.

In this paper, we present results from reprocessing the Halfmile Lake 3D seismic reflection data. Main objectives are (1) to investigate the possible diffraction signature of the deep VHMS zone and (2) to improve seismic images of shallow and deep structures. We selected a processing approach based on prestack dip moveout (DMO) and poststack migration sequence, carefully focusing on the processing steps that are critical for data acquired in crystalline environments. We show how the DMO approach used in this reprocessing has enabled us to image the diagnostic diffraction signature of the deep VHMS zone and helped facilitate a better understanding of the associated geologic structures. The results presented in this paper should help reduce risks associated with targeting deep, high-amplitude seismic anomalies for VHMS mineralization.

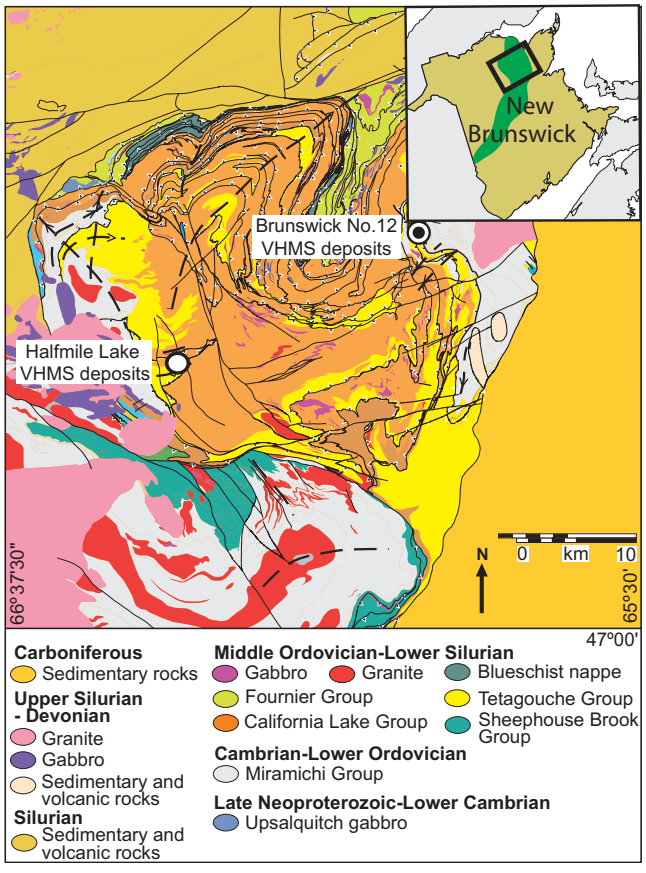

Figure 1. General geology of the Bathurst mining camp, including Halfmile Lake and Brunswick No. 12 VHMS deposits (modified from Goodfellow, 2007). The Halfmile Lake VHMS deposit is the focus of this study. The inset map shows geographical location of the Bathurst mining camp, New Brunswick, Canada.

GEOLOGIC SETTING

The Halfmile Lake deposit, with more than 25 million tons of sulfide mineralization, is located in the Bathurst mining camp in New Brunswick, Canada (Figure 1). The Bathurst mining camp is well known for its globally important VHMS deposits, such as the giant Brunswick No. 12. By the end of 1999, the Bathurst mining camp had produced approximately 128 million tons of ore, grading 2.9% lead, 6.5% zinc, 0.9% copper, and 82 g/t silver (Goodfellow, 2007). The Halfmile Lake deposit is located approximately 20 km west-southwest of the Brunswick No. 12 mine and 40 km southwest of Bathurst (Figure 1). Sulfide minerals of the Halfmile Lake deposit occur within an intensely cleaved and overturned volcano-sedimentary succession in three main zones — upper, lower, and deep — with thicknesses sometimes reaching 50 m at depth (Figure 2).

Mineralization at Halfmile Lake comprises a chalcopyrite-pyrrhotite stringer zone (mainly in forms of patches, blebs, and stringers of chalcopyrite-pyrite-pyrrhotite) structurally underlain by a lead-zinc massive sulfide zone (Figure 2). The deep zone and the area of steeply dipping stratigraphy connecting it to the lower zone are the main targets of this study (Figure 2). The deep mineralized zone consists of pyrrhotite-rich breccia-matrix sulfides and pyrite-pyrrhotite-rich layered sulfides distributed in a relatively laterally continuous sheet (Mireku and Stanley, 2007).

Structurally, the entire sequence is overturned, with a stratigraphic footwall to the massive sulfide zone dominated by quartz-feldspar

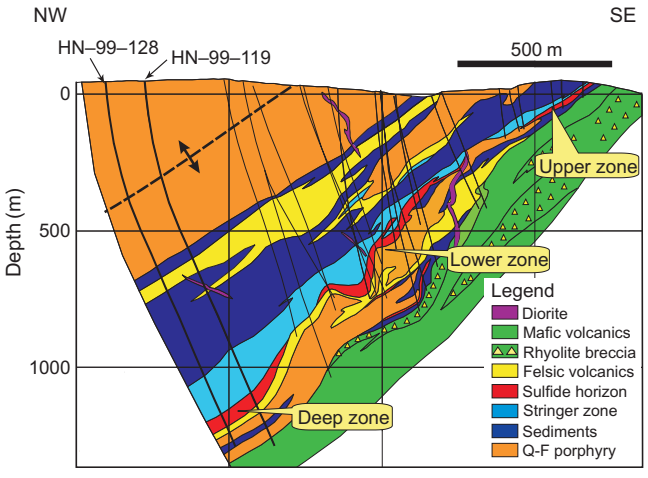

Figure 2. Composite geologic cross section through the Halfmile Lake deposit. Significant concentrations of sulfide minerals occur in three zones (upper, lower, and deep zones). The geologic cross section is published with permission from Xstrata, and the exact location is shown in plan in Figure 4a.

porphyritic (Q-F porphyry) intrusions, aphyric and porphyritic pyroclastic rocks, and fine- to coarse-grained epiclastic rocks (Figure 2). The stratigraphic hanging wall consists predominantly of felsic volcanic rocks (Thomas et al., 2000). However, mafic-ultramafic dikes and flows sometimes occur in both hanging wall and footwall (Adair, 1992). Folding of the stratigraphic sequence placed the deposit on the southern limb of an overturned antiform (Figure 2), where the average dip is about 45° to the north-northwest. However, the sulfide sheets are irregular and steepen locally because of multiple periods of fold deformation.

PHYSICAL ROCK PROPERTIES

Petrophysical measurements of P-wave velocity and densities of host rocks and mineralized zones were carried out by Noranda Inc. and the Geological Survey of Canada (Salisbury et al., 2000). Results indicated that VHMS deposits in the volcano-sedimentary setting of the Bathurst mining camp should generate high acoustic-impedance contrasts, leading to a strong seismic signature. Thus, it was believed that, with proper data acquisition, VHMS mineralization could be directly detected with seismic reflection methods. The physical rock properties of the main lithological units as well as the deep VHMS zone derived from intersecting borehole HN-99-119 are shown in Figure 3.

Synthetic traces produced by convolving the reflection coefficients with a 50-Hz Ricker wavelet indicate that the reflectivity of the host rocks above the orebody should be very weak and that these layers could be considered seismically transparent. On the other hand, the deep VHMS zone should produce a strong P-wave seismic signature (Figure 3). A comprehensive description of physical rock-property measurements from the Halfmile Lake area can be found in Salisbury et al. (2000), Matthews (2002), and Salisbury et al. (2003).

SEISMIC DATA ACQUISITION

Prior to the 3D acquisition, 2D seismic reflection surveys were conducted by Noranda Inc. over the Halfmile Lake area in 1995 and 1996. Results from one 2D survey identified a series of high-amplitude seismic anomalies and helped define the acquisition parameters required for the 3D survey (Matthews, 2002). Because of the complex structural geology of the mining camp, many of the high-amplitude seismic anomalies were thought to originate from some distance out of the plane of the 2D profile. Seismic reflection data along a different seismic profile allowed successful imaging of the lower VHMS zone (Salisbury et al., 2000), which gave Noranda Inc. great hope that a 3D survey could identify more VHMS mineralization zones.

To properly locate the origin of high-amplitude anomalies and explore more VHMS mineralization zones, a 3D dynamite survey was carried out in 1998 over a grid of approximately 18 km^2, comprising 16 shot lines perpendicular to eight receiver lines, each nearly 400 m apart (Figure 4a). In total, 1600 active channels were used during the data acquisition, with a nominal receiver interval of 20 m and shot spacing of 60 m. A total of 690 shots were fired in 9-m-deep holes using a 0.5-kg charge size. Table 1 shows the main acquisition parameters used for the 3D seismic data acquisition.

The raw shot gathers show good-quality seismic data with clear first arrivals often observed at far offsets (up to 4.5 km), potentially useful for imaging steeply dipping geologic features. Despite the presence of high-amplitude source-generated noise (e.g., shear wave, ground roll, and air blast) and occasional ambient noise (e.g., rain and wind), even weak reflections can sometimes be identified from raw shot gathers.

Figure 5 shows a typical raw shot gather recorded on all active receiver lines. Analysis of the amplitude spectrum of most shot gathers indicates that frequencies as high as 110 Hz (above −20 dB) were recorded, but the dominant frequencies range is 50–70 Hz. Near-surface velocities were generally about 5500 m/s. According to the sampling theorem for a given receiver spacing of 20 m, first arrivals would be spatially aliased above 140 Hz. Much of the low-frequency noise on shot gathers is associated with ground roll and shear-wave energy and is typically below 30 Hz. Some traces with reverse polarities were also found.

3D CDP binning

For a dipping reflector, the minimum bin size is theoretically defined from the following formula (Yilmaz, 2001):

$$\Delta x \le \frac{V_{\text{rms}}}{4 f_{\text{max}} \sin \alpha}, \tag{1}$$

where V_{rms} is the rms average of velocities down to the target reflector, f_{max} is the maximum nonaliased frequency required to resolve the target reflector, and α is the structural dip. Based on a maximum useful frequency of 80 Hz (estimated by studying amplitude spectrum), V_{rms} of 5600–6000 m/s (estimated from available sonic logs; Figure 3), and maximum dip of structures about 50°–60° (Figure 2), we estimate that a bin size range of 20–28 m would be appropriate for the Halfmile Lake 3D data. In practice, other parameters such as survey geometry affect the design of CDP bin size.

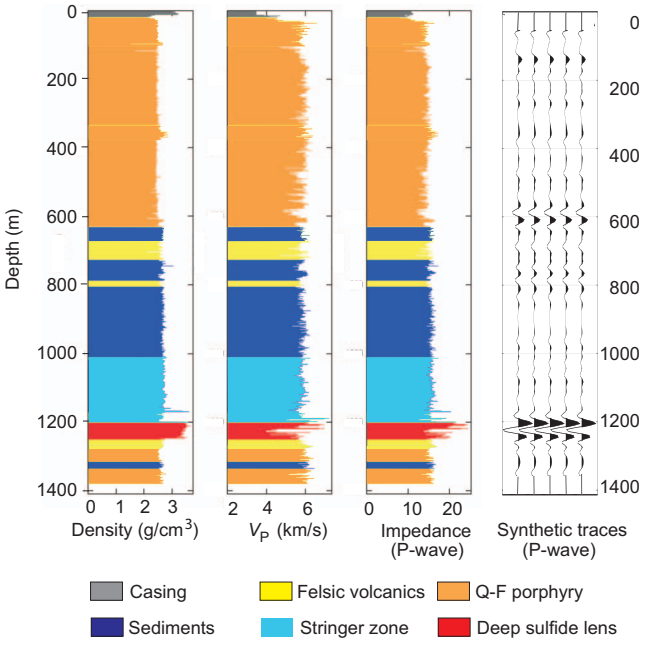

Figure 3. Density, P-wave velocity, impedance, and synthetic traces from the discovery borehole HN-99-119 shown in Figure 2 (modified from Bellefleur et al., 2004). The only significant seismic reflection is generated from the deep VHMS deposit at ~1200 m. A weak reflection on the synthetic traces at ~600 m is attributed to irregular borehole walls, not to lithological contact.

Based on a series of tests, we finally chose a CDP bin size of 25 m. This resulted in a more evenly distributed CDP fold and a slightly higher CDP fold coverage near the border of the 3D grid. The resultant CDP fold coverage is shown in Figure 4a, with the CDP fold varying from 20 to 120. Fold is high in the vicinity of the known massive sulfide lenses, near shot line 10 and receiver line 9, and is lowest near the border of the 3D grid. Figure 4b and c shows source-receiver offset distribution and azimuthal coverage for the entire 3D data set. Offsets up to 4.5 km and wide azimuth coverage are required for targeting deep-seated mineralization zones located in the steeply dipping geologic setting of the Halfmile Lake area.

3D SEISMIC DATA PROCESSING STRATEGY

The initial 3D processing of the Halfmile Lake data was carried out using a prestack migration algorithm based on the assumption that sheet-like VHMS deposits in the Halfmile Lake area should produce strong reflections. This strategy was validated with the discovery of the deep VHMS zone. The choice initially was guided by the consideration that economically viable deep-VHMS mineralization would be sufficiently large and, thus, produce significant reflectivity that would show up on a prestack migration volume. Our processing and imaging strategy involved a prestack DMO and poststack migration. Similar processing flows have been effective in 2D and 3D seismic reflection studies in crystalline environments (e.g., Milkereit et al., 1996; Adam et al., 2003). DMO stack processing preserves diffraction signals that might originate from zones of mineralization.

Table 2 shows the principal processing steps used to reprocess the Halfmile Lake data. Because of their importance, some of the key processing steps are detailed in the following subsections.

Prestack filtering strategy

Figure 6 shows the increase in signal-to-noise ratio (S/N) for a sample shot gather recorded on one receiver line after various processing steps. Frequency and surface-consistent deconvolution filters were designed to preserve the highest frequency content with useful signal. A surface-consistent spiking deconvolution using a 100-ms operator length helped to improve resolution and to compensate for the effects of variable coupling conditions caused by the sources and receivers being placed on exposed bedrock or overburden (Figure 6b). Part of the direct shear-wave energy was reduced in the shot gathers after implementing the band-pass filter and surface-consistent deconvolution. Remaining direct shear waves, in a few shot gathers, were muted subsequently at near offsets and attenuated at far offsets (>2000 m) using a median filter.

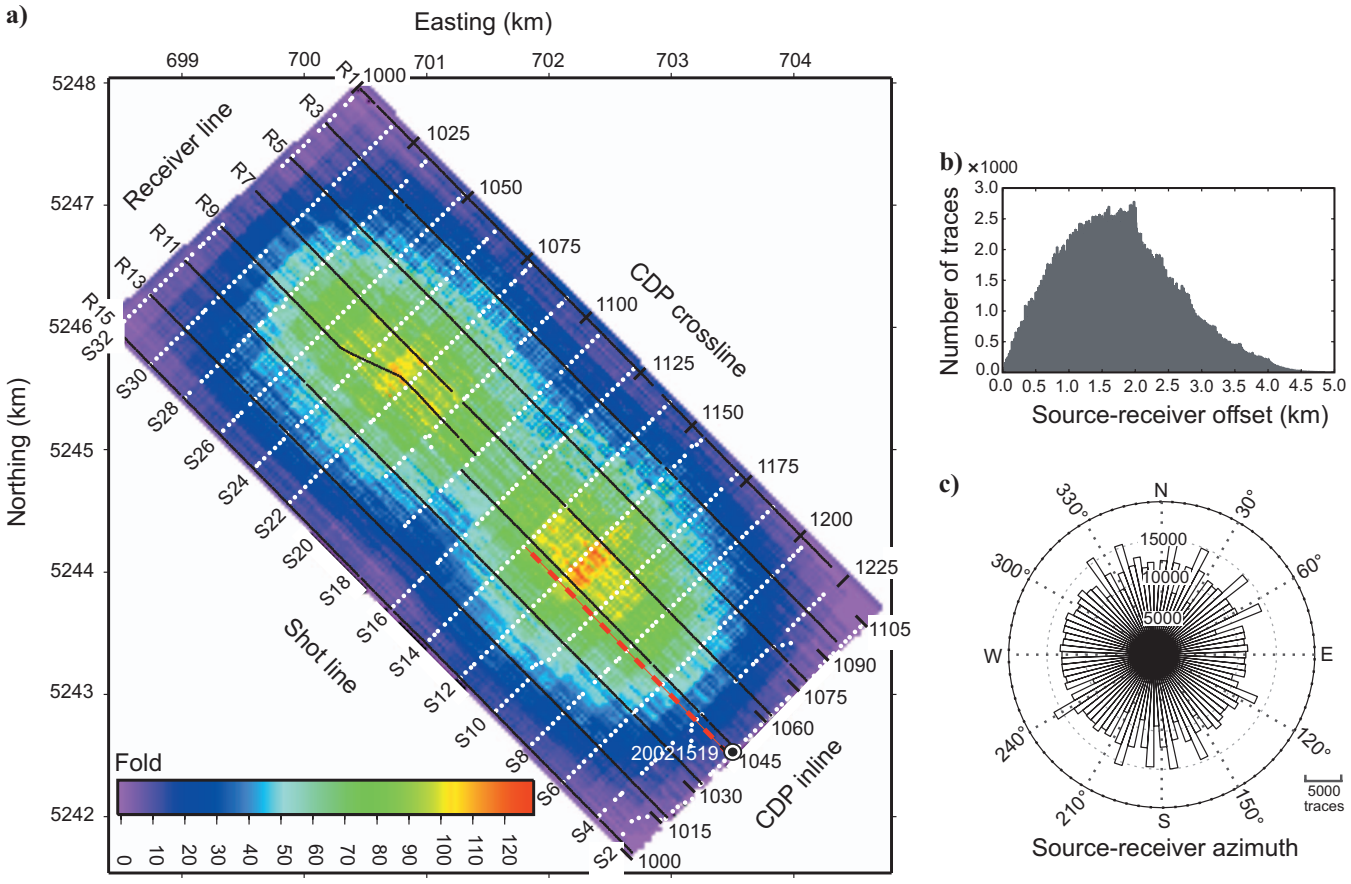

Figure 4. (a) 3D seismic reflection shots (white dots) and receivers (solid black lines) acquisition geometry projected onto CDP fold coverage calculated from a CDP bin size of 25 m. The thick black dot in (a) marks the location of raw shot gather 20021519 shown in Figure 5. Shown also are the system of CDP inlines and crosslines used for the 3D processing. The dashed red line shows the exact location of the geologic cross section shown in Figure 2. (b, c) Source-receiver offset distribution and azimuth coverage from the 3D survey. Traces within each 4° azimuth sector are grouped together for display purposes.

Refraction static corrections

Obtaining an accurate refraction weathering static solution is critical to effective seismic imaging in crystalline environments. To calculate refraction static corrections, we picked first arrivals using an automatic neural network algorithm from the entire data set; later, we manually inspected and corrected where needed. The 3D refraction static corrections were calculated based on approximately 1,050,000 repicked first arrivals. Resulting source and receiver static corrections, including the effects of large topographic variations, varied from 0 to 80 ms. Near-surface traveltime distortions were largely removed after applying refraction static corrections, and the coherency of reflections improved markedly (Figure 6c).

The first arrivals were further used to design a gentle trace-top mute function to remove the direct P-wave and refracted energy (Figure 6d) and to preserve, as much as possible, wide-angle reflections/diffractions and the near-surface reflections that can be linked with surface geology.

Normal-moveout (NMO) and DMO corrections

In crystalline environments such as the Halfmile Lake area, lithological contacts are often complex, steeply dipping, discontinuous, deformed, altered, and folded (Figure 2). In such environments, reflectors are often of limited lateral extent with various dips and sometimes behave as point scatterers rather than continuous specular reflectors (Schmelzbach et al., 2007). There is no velocity function for normal-moveout (NMO) corrections that will simultaneously optimize stacking of dipping and subhorizontal reflections. Anomalously higher stacking velocities are necessary to allow dipping reflections to stack correctly. Even then, reflectors with one dip are often enhanced at the expense of other conflicting reflectors with different dips (Hale, 1991). DMO corrections allow conflicting reflections with various dips to stack simultaneously using the background interval velocity (Deregowski, 1986).

We used a 3D Kirchhoff integral DMO method based on Hale (1991) to compute the DMO-corrected 3D stack volume. DMO velocities range from 5650 to 5900 m/s. Figure 7a shows an unmigrated stacked section along inline 1060 obtained using only NMO corrections. Figure 7b shows a significantly improved version of the same inline after NMO and DMO corrections. By increasing the S/N and allowing simultaneous imaging of conflicting seismic events, the DMO process clearly allowed the imaging of diffraction D1, and reflection R1 and improved continuity of a series of steeply dipping reflections in the southeastern part of the section (Figure 7b).

Table 1. Main acquisition parameters for the Halfmile Lake 3D seismic survey, 1998.

Survey parameters	
Recording system	SERCEL 388
No. of receiver lines	8 lines: R1,R3,…,R15
No. of shot lines	16 lines: S2,S4,…,S32
Receiver-line interval	406 m
Shot-line interval	406 m
Maximum source-receiver offset	4870 m
Survey area	~18 km^2
Source	Dynamite
CDP bin size	25 m (inline and crossline directions)
Spread parameters	
Receiver spread array	8 lines × 201 active channels
Receiver (group) interval	20 m
Source interval	60 m
Recording length	3 s
Sampling rate	2 ms
Receiver and source parameters	
Geophone type	Sensor SM-4
Geophone frequency	14 Hz
Type of base	7.5 cm spike
No. of geophones per set	6 over 1.0 m
Geophone separation	0.2 m linear
Source pattern	Single hole
Shot depth	9 m
Charge size	0.5 kg
No. of shots	690

Poststack filtering and migration

Deconvolution in the space-frequency domain f_{xy} was implemented as a poststack coherency filter to suppress random noise. We used a short 19 × 19 trace filter and a short 80-ms window to preserve short reflections as well as curved events such as diffractions. This noticeably enhanced continuity of reflections and diffractions.

We tested several poststack migration algorithms with the aim of collapsing the diffraction (i.e., D1 in Figure 7b) into a localized area. In particular, we compared results from Stolt (1978), phase-shift (Gazdag, 1978), and finite-difference (Yilmaz, 2001) migrations applied using a smoothed version of the stacking velocities. Our analysis shows that the diffraction is best collapsed with the 45° finite-difference migration algorithm. However, steeply dipping reflections were best preserved with phase-shift migration. The smoothed ver-

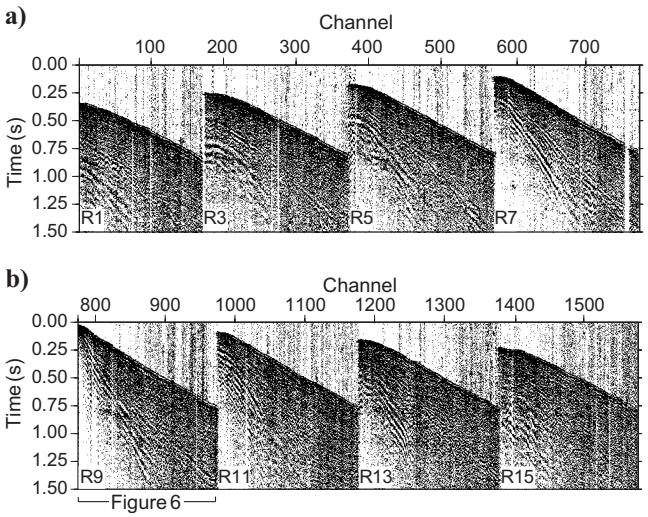

Figure 5. A raw shot gather (20021519) recorded into (a) receiver lines R1 to R7 and (b) receiver lines R9 to R15. A closeup of the data along receiver line 9 (R9) is shown in Figure 6a.

sion of the stacking velocity field used for migration was also used for the time-to-depth conversion. The smoothed velocity field is consistent with the well-log velocities within ±5% (Figure 3).

IMAGING RESULTS AND INTERPRETATION

Subsurface structures are well imaged in the unmigrated cube from ~250 ms down to ~1000 ms. Reprocessing results reveal several steeply dipping reflections, some of which can be linked to known geology. Moreover, our results indicate that diffractions, a highly diagnostic VHMS deposit signature, are obtained only by using a DMO stack processing approach. The following interpretation results are based on unmigrated and migrated 3D volumes.

Assessment and limitation of resultant image

Before we begin our interpretation of the obtained results, it is important to investigate the required lateral and vertical extent of a VHMS deposit for it to be fully resolved and detected in the Halfmile Lake 3D data set. The dominant frequency of the final 3D unmigrated cube is within the 50–70-Hz range. Using the Rayleigh quarter-wavelength criterion (Widess, 1973) for an assumed given average velocity of 5800 m/s, the vertical resolution (minimum vertical extent) is 20–30 m. Using the Fresnel zone criterion (e.g., Sheriff and Geldart, 1995; Yilmaz, 2001) for given depths of 1000 and 1500 m (~0.35 and ~0.5 s), the horizontal resolution varies between 200 and 250 m, and 250 and 300 m, respectively. Migration tends to collapse the Fresnel zone to approximately the dominant wavelength (Stolt and Benson, 1986). However, the presence of noise and migration-velocity errors affects migration adversely and can degrade the horizontal resolution significantly. VHMS deposits smaller than the Fresnel zone can still be detected but might not be fully resolved (Salisbury and Snyder, 2007).

Based on the Rayleigh scattering theory (Korneev and Johnson, 1993), the minimum lateral extent of a detectable VHMS deposit is $\lambda/2\pi$, where λ is the dominant wavelength. For the Halfmile Lake 3D data, the minimum lateral extent is 13–18 m at depths of 1000–1500 m. However, this detection criterion does not take into account that objects smaller than the Fresnel zone normally lead to scattered energy that diminishes rapidly at deeper origins (Berryhill, 1977). Because the amplitudes from VHMS deposits are very strong (Salisbury et al., 2003), we think that this rapidly decreasing energy will not necessarily prevent the imaging of the diffractions. Therefore, delineating a 13- to 18-m-wide orebody might be possible but will likely depend on noise conditions.

Table 2. Principal processing steps applied to the full 3D data set, 2009.

Step	Parameters
1	Read 1.5 s SEG-Y data
2	Extract and apply geometry (several tests for CDP bin size)
3	Trace editing and polarity reversal
4	Pick first breaks: full offset range, automatic neural network algorithm but manually inspected and corrected
5	Refraction static corrections: datum 500 m, replacement velocity 5600 m/s, V_0 1000 m/s
6	Geometric-spreading compensation: V^2t
7	Band-pass filtering: 20–30–90–110 Hz
8	Surface-consistent deconvolution: filter 100 ms, gap 14 ms, white noise 0.1%
9	Top mute: 35 ms after first breaks
10	Direct shear-wave muting (near offset) or attenuation (far offset)
11	Air blast attenuation
12	Trace balance using data window
13	Velocity analysis (iterative): every fourth CDP inline and fifth crossline
14	Residual static corrections (iterative)
15	NMO: 50% stretch mute
16	3D DMO corrections (iteratively link to velocity analysis)
17	Stack
18	f_{xy} deconvolution: inline and crossline directions
19	Trace balance: 0–1300 ms
20	Migration: using smoothed stacking velocities, 45° 3D finite difference (for diffraction signal from the deep zone) and 3D phase shift (for steeply dipping reflections)
21	Time-to-depth conversion: using smoothed stacking velocities

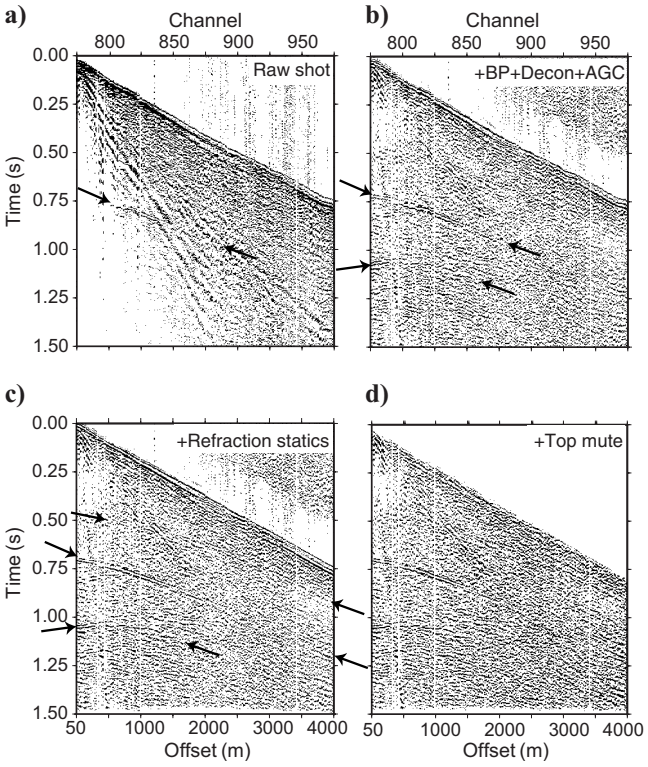

Figure 6. A closeup of the raw shot gather 20021519 (see also Figure 5) for the data recorded along receiver line 9 (R9), showing data quality and improvement in S/N after different processing steps (a-d). Note the increase in coherency and S/N for reflections shown with black arrows. Automatic gain control has been applied for display purposes.

Scattering signature of the deep VHMS deposit

Processing results show several high-amplitude anomalies on the unmigrated and migrated seismic cubes. Figure 8 shows a set of slices from the unmigrated cube, indicating the presence of a pronounced diffraction in inline 1060, a concentric diffraction from a time slice at 440 ms, and a strong steeply dipping event in crossline 1154. All of these constitute the seismic response from the deep VHMS zone. In the time slice, the strong diffraction covers a region with radius of about 600 m (Figure 8a), considerably larger than the estimated lateral extent of the deep VHMS lens (~200 m). The strongest amplitudes along the diffraction hyperbola are found north of the apex, indicating that the deep VHMS lens dips to the north. This agrees with the geometry of the deep VHMS lens defined from about nine boreholes.

More important, however, is the asymmetric shape of the diffraction relative to the location of the deep VHMS zone. The true location of the deep VHMS lens is not located in the center of the semicircular diffraction pattern. This is particularly clear on the time slice and confirms that the deep VHMS lens produces complex scattering that cannot be approximated by a point scatterer. A careful observation of the unmigrated time slices also reveals that two short segments of the semicircular diffraction have near-zero amplitude (nodes P1 and P2 in Figure 8a). These two small segments separate the strongest amplitudes of the deep VHMS zone diffraction signal on the northern side from the weaker amplitudes in the southern side. We interpret that the asymmetric-response and zero-amplitude segments, two important seismic characteristics of the deep zone, are likely related to the shape of the deep VHMS lens.

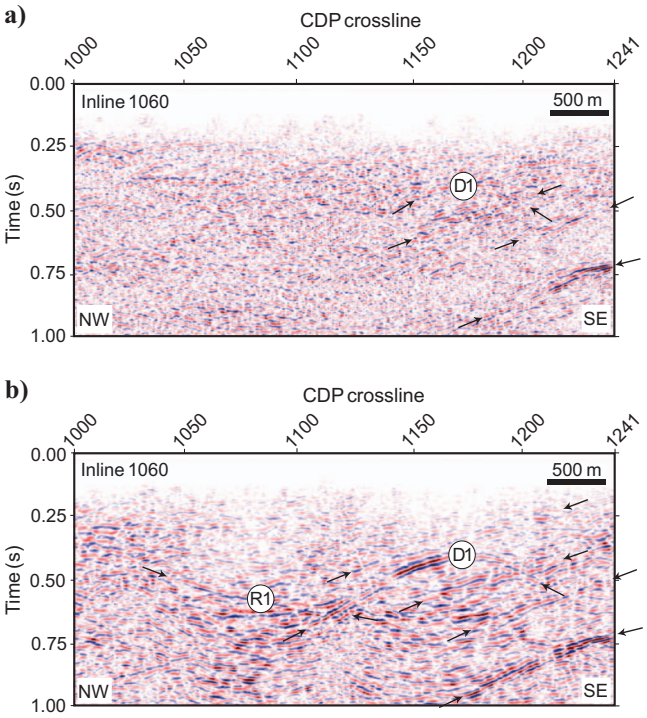

Figure 7. Unmigrated seismic section from inline 1060 with (a) only NMO corrections applied and (b) NMO and DMO corrections applied, demonstrating improvements in the continuity of several steeply dipping reflections in the southeastern side of the section and allowing imaging of reflections R1 and diffraction D1 originating from the deep VHMS deposit.

Figure 9 shows a collapse of the diffraction on a set of slices from the migrated cube. The diffraction is best focused into a localized bright spot at a depth about 1200 m (Figure 9a and b). An apparent north-northeast dip of the deep VHMS zone is clearly observed from the migrated image in the crossline section (Figure 9c). The migrated cube was converted to depth and visualized with the existing 3D geologic model of the deep VHMS lens to confirm the correspondence between the strong amplitudes and the deep zone (Figure 10). The strong amplitude anomaly is located exactly at the location of the deep VHMS zone as intersected by discovery borehole HN-99-119 (Figure 10).

Host-rock structures

Interpretation of geologic structures from seismic reflection data acquired in crystalline environments is often ambiguous and challenging because of complex geology, i.e., rocks are strongly metamorphosed, altered, folded, and deformed at several stages. Here, we used existing geologic information to reduce the ambiguity and focused our interpretation in the southern part of the 3D cube, where most of the support data are found. Lithological intersections in boreholes and physical rock properties were the key to the interpretation of the host-rock structures. We conducted the interpretation based on the unmigrated seismic volume, mainly because this stack volume contains dipping reflectors located on the margins of the cube, which slightly moved outside the cube after migration.

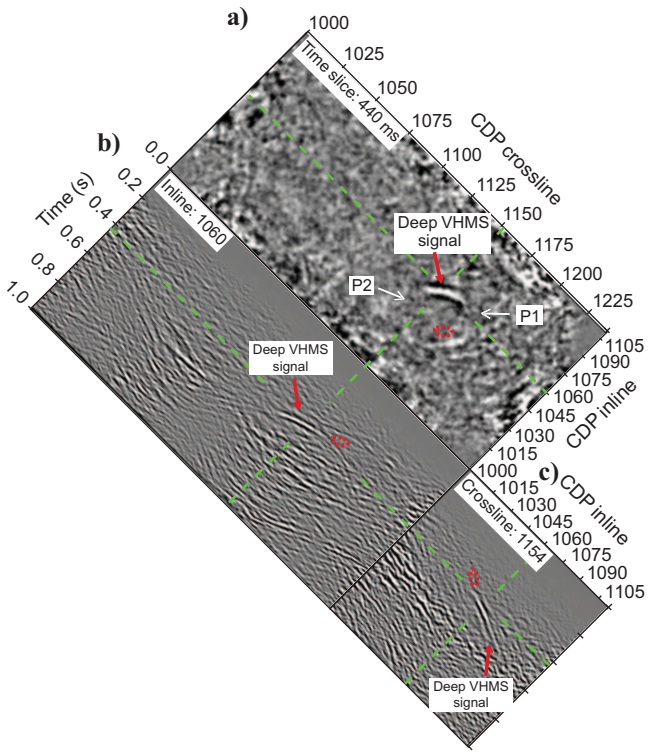

Figure 8. Unmigrated data from the Halfmile Lake 3D seismic data, showing (a) a time slice at 440 ms, (b) inline 1060, and (c) crossline 1154. Red arrows mark location of the strong diffraction signal originating from the deep VHMS deposit. The highest amplitude occurs on the northern flank of the diffraction, confirming that the deep VHMS deposit dips approximately in this direction. Red dotted region on (a)–(c) marks the projected location of the deep VHMS zone.

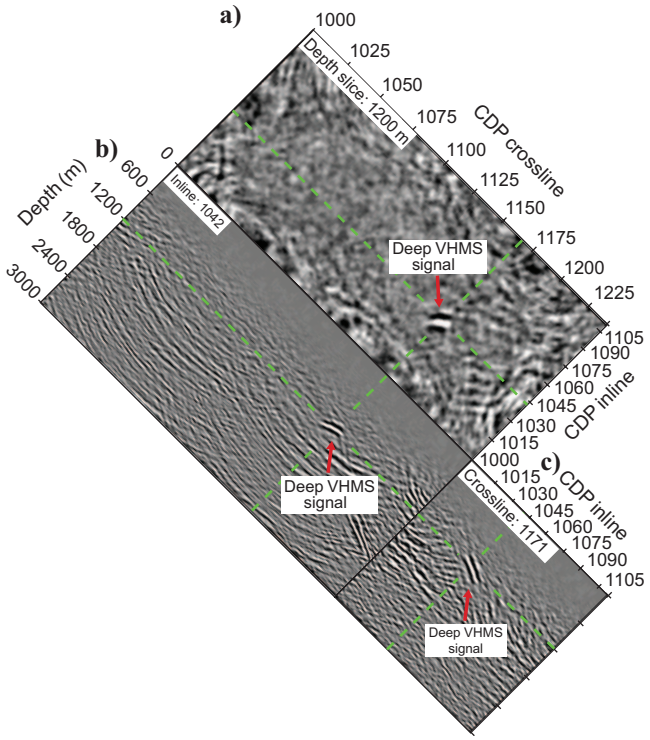

Figure 9. Migrated data from the Halfmile Lake 3D seismic data, showing (a) a depth slice at 1200 m, (b) inline 1042, and (c) crossline 1171. The depth slice (a) shows the successful collapse of the diffraction signal observed in Figure 8 into a localized bright spot, which corresponds to the location of the deep VHMS lens.

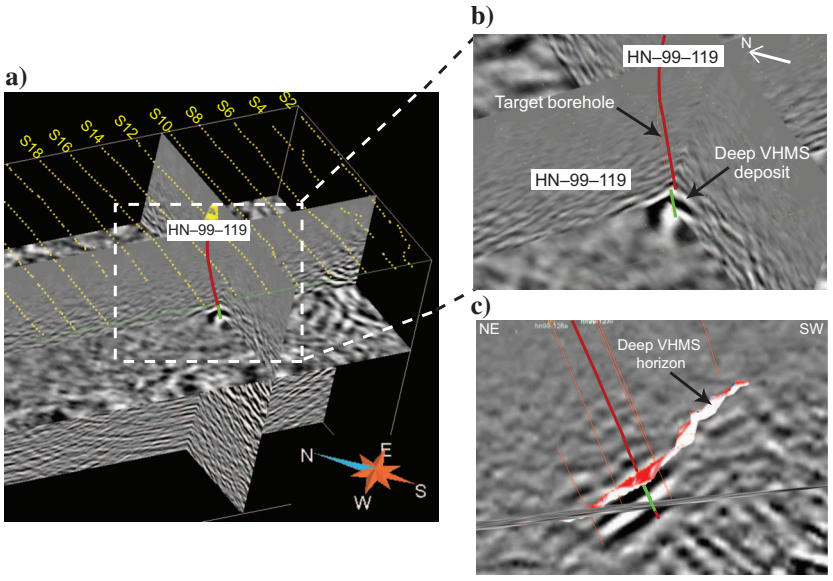

Figure 10. (a-c) Composite 3D perspective views from migrated slices, showing how high amplitudes in the seismic data correlate with the location of the deep VHMS deposit at 1.2 km depth. Solid green line in (a-c) marks the intersection of the borehole HN-99-119 with the deep VHMS zone. $V = H$.

The first 1.0 s of the stacked data comprises two main reflectivity patterns. Near-surface structures down to about 1500 m (~0.5 s in the unmigrated cube) are relatively transparent, except in the southeastern parts and near the deep VHMS lens. Strong reflections are observed at depths greater than 1500 m (Figures 7b and 8). The analysis of inline and crossline sections helps to interpret structures associated with the VHMS deposits and the two main reflectivity patterns.

Figures 11 and 12 show a series of inline and crossline sections from the southeastern and northwestern parts of the unmigrated cube. Five sets of reflections and/or reflectivity patterns can be identified, including R1 nearly flat lying in inline and crossline sections (Figures 7 and 11), R2 with a gentle apparent dip to the northwest in inline sections and a steeper apparent dip to the northeast in crossline sections, and three steeply northwest-northeast-dipping reflections in inline and crossline sections (black arrows, Figures 11 and 12).

By comparing the crossline and inline sections, we conclude that the three steeply dipping reflections in the southeastern part of the unmigrated cube have a true dip direction to the north — a dip direction that generally corresponds to the dip of the main lithological units in this part of the cube. Reflection R2 mainly dips to the northwest, with a different angle to the main known lithological contacts (see Figures 11 and 12). The strong amplitudes of this reflection indicate that it originates from a contact with a high acoustic-impedance contrast. In the absence of borehole data at this depth (~2−2.5 km), we attribute R2 to a dioritic intrusion, known to exist in the Halfmile Lake area (Thomas et al., 2000). Mafic to ultramafic dikes and/or intrusions from similar geologic environments elsewhere in the world are known to produce similar continuous high-amplitude seismic reflections (e.g., Juhlin et al., 1990; Malehmir et al., 2007; Malehmir et al., 2009).

Further analyses of inline sections help to mark a weak reflectivity pattern in a region located just above the highest amplitude of the diffraction signal originated from the deep zone (see Figures 2 and 12). Physical rock-property measurements on samples indicate that the sulfide stringer zone has an acoustic-impedance contrast with all of the lithological units and could produce a reflection. Based on this and on their spatial correspondence, we attribute the weak reflectivity to the stringer zone.

Rock-property measurements on samples indicate that the Q-F porphyry or rhyolite tuff units (felsic volcanics) in contact with mafic volcanic rocks or sediments could produce a detectable reflection. These lithological contacts are possible explanations for the steeply dipping reflections observed in the southeastern part of the unmigrated cube (see Figures 2 and 12). The Q-F porphyry-sediment contact can also explain reflection R1, which is well defined and quite extensive in the northern part of the cube (Figures 7b and 11). If so, then R1 marks the position of this contact on the northern limb of the Halfmile Lake anticline. The Q-F porphyry-sediment contact is particularly important for exploration in the Halfmile Lake area because it is often associated with sulfide mineralization.

Seismic signature of the lower VHMS zone

A short, high-amplitude reflection observed on the unmigrated inline sections 1058 and 1059 (Figure 12) suggests a change of dip and a localized thickening of the VHMS horizon above the weak reflection near 0.25 s. This short, high-amplitude reflection (L_1) appears on a few more inline and crossline sections near the known location of the lower VHMS zone. The exact position of L_1 cannot be determined precisely because it is not preserved on the migrated data. However, this depth location also coincides with a strong reflection attributed to the lower zone from a high-resolution 2D seismic survey previously conducted in the study area (Salisbury et al., 2000). Thus, we interpret the short reflection L_1 as the seismic signature of the lower VHMS zone. Previous processing results of the 3D Halfmile Lake data set did not allow imaging the lower VHMS zone (see Matthews, 2002).

DISCUSSION

Several studies have been undertaken to investigate the seismic response of VHMS deposits, either with numerical modeling (e.g., Eaton, 1999; Bohlen et al., 2003) or from case studies over known deposits (e.g., Milkereit et al., 2000; Salisbury et al., 2000; Adam et al., 2003). These studies have shown that a typical VHMS deposit should produce a diagnostic diffraction response, with the scattering directivity controlled primarily by shape and secondarily by the composition of the orebody. For example, numerical simulation of a scattered wavefield using elastic finite-difference methods predicts that a dipping lenticular sulfide lens will produce diffractions with high amplitudes in the downdip direction (Bohlen et al., 2003).

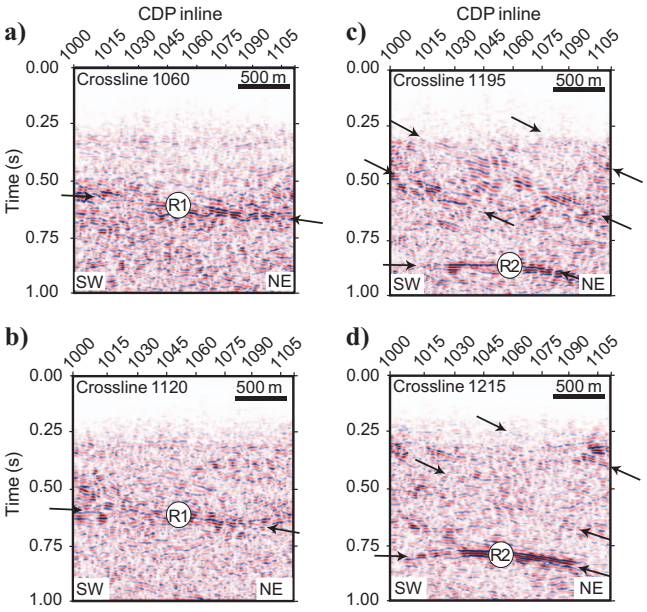

Figure 11. Unmigrated seismic sections from crosslines (a) 1060, (b) 1120, (c) 1195, and (d) 1215, showing two gently to subhorizontal north-dipping reflections (R1 and R2) and three shallow steeply north-dipping reflections marked with black arrows in (c) and (d). Reflection R2 is attributed to a major dioritic intrusion because of its strong amplitude and discordant dip to the main lithological contacts. Reflection R1 is attributed to the northern flank of the main anticlinal structure and the steeply dipping reflections are attributed to the contacts between Q-F porphyry and sedimentary rocks.

The modeling results also predict changes in phase-reversal positions with respect to the phase of the normal-incidence wave. The change in phase reversal positions is interpreted as caused by the composition effect, irrespective of the shape of orebody (Bohlen et al., 2003). In theory, the recognition of phase changes could serve as a diagnostic tool to estimate the composition of an orebody and might increase drilling success rates. Previous experience with high-resolution seismic reflection surveys over crystalline environments indicates that the typical low S/N of the data acquired in these environments makes identification of phase changes difficult, even with careful processing. With the Halfmile Lake 3D data set, D1 is identified on at least three receiver lines for a limited number of shot gathers, but a phase reversal cannot be identified. The time slice of the unmigrated data shown in Figure 8a suggests phase reversal, or at least two zero-amplitude segments (P1 and P2) that could be associated with phase reversal.

It is difficult to explain how a phase reversal would be preserved after stacking, but it might be imaged if the highest amplitude of the diffraction originates from shots within a specific azimuth. This possibility is supported by a preliminary azimuthal analysis of the contribution of shots and receivers. However, it is unclear what phase reversal can be expected from an orebody comprising different sulfide minerals, each having slightly different phase-reversal characteristics. Because of this and the strong asymmetric diffraction signature, we prefer to explain the zero-amplitude segments by a combined effect of orebody shape and acquisition geometry. However, this also might be the first case study identifying a phase reversal from the data acquired over crystalline environments. Therefore, our results demonstrate that the ability to preserve diffraction and potentially

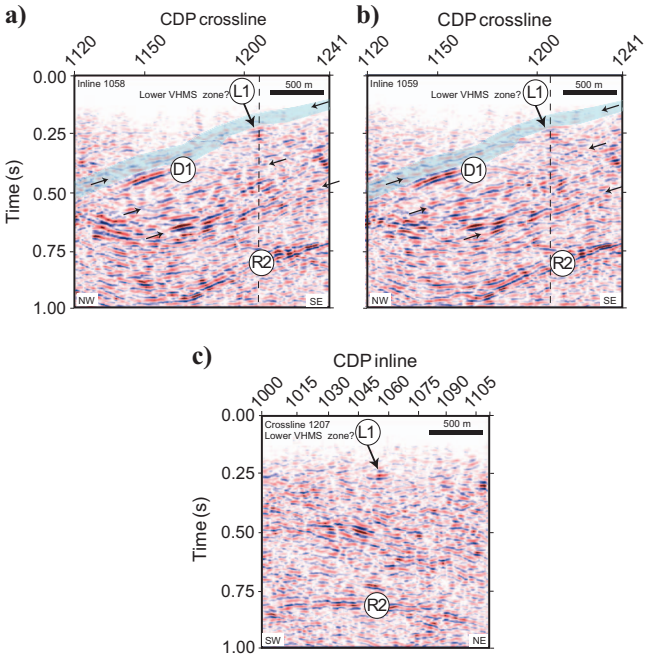

Figure 12. Unmigrated seismic sections extracted from the stacked cube in inlines (a) 1058, (b) 1059, and (c) crossline section, showing a short segment of high-amplitude reflection (L1) imaged at ~0.25 s. The L1 reflection is attributed to part of the Lower VHMS zone. The blue area in (a) and (b) above reflection L1 and diffraction D1 is interpreted to represent the stringer zone. Dashed lines in (a) and (b) mark the location of the crossline 1207 shown in (c).

the phase reversal related to the composition of VHMS deposits is best when using a prestack DMO approach.

Comparison of unmigrated inline sections and time slices indicates that the diffraction from the deep zone is asymmetric not only in terms of amplitude variations but also relative to the true location of the deep VHMS lens, meaning that the diffraction apex does not mark the location of the sulfide lens (Figure 8). Similar situations have been examined by Bohlen et al. (2003) through 3D finite-difference modeling. They conclude that the scattering center lies at areas with strong curvature first reached by the incident P-wave. Eaton (1999) explains this by a tendency of lenticular VHMS bodies to produce diffracted seismic energy in a narrowly focused region in the downdip direction. Earlier, Berryhill (1977) shows that the highest amplitude of a diffraction from the edge of a short dipping reflection occurs where the diffraction meets the reflection, which is not at the apex of the diffraction hyperbola.

A similar asymmetric diffraction response has been reported from a 3D seismic survey conducted on a known deep nickel/copper deposit in the Sudbury impact structure (Milkereit et al., 2000). The asymmetric diffraction signature of the deep VHMS zone and the strong amplitude variations with offset (AVO) and azimuth (Figure 8) highlight the need to be cautious when selecting diffraction imaging algorithms to locate the spatial origin of diffractions. In particular, methods based on unmigrated stacked data and calculating coherency along traveltime trajectories corresponding to point scatterers would provide invalid results for a scatterer like the deep VHMS deposit (e.g., Gersztenkorn and Marfurt, 1999 and references therein; Fomel et al., 2007; Moser and Howard, 2008).

It is also fundamentally important to remove source-generated and ambient noise prior to stacking before making any analysis based on the shape of the diffraction. The weaker part of the concentric diffraction pattern in the updip direction (Figure 8) could be missed without sufficient S/N. In such a case, the strong part of the diffraction in the downdip direction could be misinterpreted as a specular reflection (Eaton, 1999). Therefore, the identification of such a diffraction could be clearly ambiguous not only on 2D profiles (Eaton, 1999) but also on 3D data, especially if they do not exhibit the complete circular pattern in a time slice, as shown in Figure 8a.

CONCLUSIONS

The Halfmile Lake area is a clear example of a steeply dipping and strongly deformed, folded, and altered crystalline environment. Despite this geologic and structural complexity, our results demonstrate that with careful selection of data acquisition and processing parameters, the 3D seismic reflection method can provide useful information on the host-rock structures and can directly target VHMS mineralization. Key processing steps include refraction static corrections, pre- and poststack noise removal, and DMO corrections. The DMO stacked data have been instrumental in highlighting the diagnostic large diffraction signature of the deep VHMS deposit. Despite the advantages of a prestack migration algorithm to image complex structures, preserving the diffraction signal — a common diagnostic of VHMS orebodies — is not achievable using prestack migration.

The diffraction signal from the deep VHMS deposit displays remarkable characteristics:

- amplitude variations along the diffraction, with the highest amplitudes occurring at the northern flank of the diffraction, an indication that the deep VHMS deposit mainly dips to the north
- large and asymmetric semicircular diffraction signature relative to the location of the deep zone, indicating that the deep VHMS deposit does not lie at the center of the diffraction in time slices or on the apex in inline sections
- two zero-amplitude segments that might be an indication of phase reversal or an effect from the shape of the VHMS deposit

Our findings suggest that the remote detection and delineation of a lenticular-shaped VHMS deposit similar to the deep VHMS lens would only be possible using 3D seismic surveys.

Successful removal of direct P- and S-wave energy has allowed correlation of most shallow reflections with known lithological contacts and has helped to identify a short segment of high-amplitude reflection in some inline and crossline sections, which we interpret to originate from the lower VHMS zone. Previous processing work did not image this zone. In addition, available petrophysical measurements such as density and P-wave velocity from the host-rock structures as well as borehole data have enabled a reliable interpretation of major reflections. Overall, five prominent reflections have been identified and related to a stringer zone, the Q-F porphyry sediments, and/or mafic-ultramafic intrusions. The strong signature of the VHMS orebody on the reprocessed cube should encourage geophysicists to explore mining camps where massive sulfides occur at key lithological contacts that extend to depth.

ACKNOWLEDGMENTS

The authors thank Larry Matthews and Sharon Taylor for discussions at early stages of reprocessing and for help in recovering raw field data, support data, and final seismic volume of the Bathurst mining camp. A. Malehmir wishes to thank the Geological Survey of Canada (GSC) and the Natural Sciences and Engineering Research Council of Canada (NSERC) for providing funds during his research Visiting Fellowship at GSC. Seismic data processing was accomplished using GLOBE Claritas™. GMT from Paul Wessel and Walter H. F. Smith and Seismic Unix from Colorado School of Mines were used to prepare some of the figures. Initial prestack migration processing results conducted by Noranda Inc. (now Xstrata) are proprietary. B. Roberts and D. Snyder provided useful suggestions to early versions of the manuscript. N. Stolz and B. Milkereit along with associate editor M. Asten are gratefully thanked for thorough and constructive reviews. This is Geological Survey of Canada contribution 20080443.

REFERENCES

Adair, R. N., 1992, Stratigraphy, structure, and geochemistry of the Halfmile Lake massive-sulfide deposit, New Brunswick: Exploration and Mining Geology, **1**, 151–166.

Adam, E., B. Milkereit, G. Arnold, and R. Pineault, 1996, Seismic response of the Bell Allard orebody, Matagami, Quebec: 66th Annual International Meeting, SEG, Expanded Abstracts, 634–637.

Adam, E., G. Perron, G. Arnold, L. Matthews, and B. Milkeriet, 2003, 3D seismic imaging for VMS deposit exploration, Matagami, Quebec, *in* D. W. Eaton, B. Milkereit, and M. H. Salisbury, eds., Hardrock seismic exploration: SEG, 229–246.

Adam, E., G. Perron, B. Milkereit, J. Wu, A. J. Calvert, M. Salisbury, P. Ver-

paelst, and D. J. Dion, 2000, A review of high-resolution seismic profiling across the Sudbury, Selbaie, Noranda, and Matagami mining camps: Canadian Journal of Earth Sciences, **37**, 503–516.
Bellefleur, G., C. Müller, D. Snyder, and L. Matthews, 2004, Downhole seismic imaging of a massive sulfide orebody with mode-converted waves, Halfmile Lake, New Brunswick, Canada: Geophysics, **69**, 318–329.
Berryhill, J. R., 1977, Diffraction response for nonzero separation of source and receiver: Geophysics, **42**, 1158–1176.
Bohlen, T., C. Müller, and B. Milkereit, 2003, Elastic wave scattering from massive sulfide orebodies: On the role of composition and shape, *in* D. W. Eaton, B. Milkereit, and M. H. Salisbury, eds., Hardrock seismic exploration: SEG, 70–89.
Deregowski, S. M., 1986, What is DMO?: First Break, **4**, 7–24.
Drummond, B. J., B. R. Goleby, A. G. Goncharov, L. A. I. Wyborn, and T. MacCready, 1997, Crustal-scale structures in the Proterozoic Mount Isa Inlier of north Australia: Their seismic response and influence on mineralization: Tectonophysics, **288**, 43–56.
Eaton, D. W., 1999, Weak elastic-wave scattering from massive sulfide orebodies: Geophysics, **64**, 289–299.
Eaton, D. W., B. Milkereit, and M. Salisbury, 2003, Seismic methods for deep mineral exploration: Mature technologies adapted to new targets: The Leading Edge, **22**, 580–585.
Fomel, S., E. Landa, and M. T. Taner, 2007, Poststack velocity analysis by separation and imaging of seismic diffractions: Geophysics, **72**, no. 6, U89–U94.
Gazdag, J., 1978, Wave equation migration with the phase-shift method: Geophysics, **43**, 1342–1351.
Gersztenkorn, A., and K. J. Marfurt, 1999, Eigenstructure-based coherence computations as an aid to 3D structural and stratigraphic mapping: Geophysics, **64**, 1468–1479.
Goodfellow, W. D., 2007, Metallogeny of the Bathurst Mining Camp, northern New Brunswick, *in* W. D. Goodfellow, ed., Mineral Deposits of Canada: A synthesis of major deposit types, district metallogeny, the evolution of geological provinces, and exploration methods: Geological Association of Canada, Mineral Deposits Division, Special Publication 5, 449–469.
Hale, D., 1991, A nonaliased integral method for dip moveout: Geophysics, **56**, 795–805.
Juhlin, C., 1990, Interpretation of the reflections in the Siljan Ring area based on the results from the Gravberg-1 borehole: Tectonophysics, **173**, 345–360.
Korneev, V. A., and L. R. Johnson, 1993, Scattering of elastic waves by spherical inclusions — II, Limitations of asymptotic solutions: Geophysical Journal International, **115**, 251–263.
Malehmir, A., H. Thunehed, and A. Tryggvason, 2009, The Paleoproterozoic Kristineberg mining area, northern Sweden: Results from integrated 3D geophysical and geologic modeling, and implications for targeting ore deposits: Geophysics, **74**, no. 1, B9–B22.
Malehmir, A., A. Tryggvason, C. Juhlin, J. Rodriguez-Tablante, and P. Weihed, 2006, Seismic imaging and potential field modeling to delineate structures hosting VHMS deposits in the Skellefte ore district, northern Sweden: Tectonophysics, **426**, 319–334.
Malehmir, A., A. Tryggvason, H. Lickorish, and P. Weihed, 2007, Regional structural profiles in the western part of the Palaeoproterozoic Skellefte ore district, northern Sweden: Precambrian Research, **159**, 1–18.
Matthews, L., 2002, Base metal exploration: Looking deeper and adding value with seismic data: Canadian Society of Exploration Geophysicists Recorder, **27**, 37–43.
Milkereit, B., E. K. Berrer, A. R. King, A. H. Watts, B. Roberts, E. Adam, D. W. Eaton, J. Wu, and M. H. Salisbury, 2000, Development of 3-D seismic exploration technology for deep nickel-copper deposits — A case history from the Sudbury basin, Canada: Geophysics, **65**, 1890–1899.
Milkereit, B., D. W. Eaton, J. Wu, G. Perron, M. H. Salisbury, E. Berrer, and G. Morrison, 1996, Seismic imaging of massive sulphide deposits: Part II, Reflection seismic profiling: Economic Geology, **91**, 829–834.
Mireku, L. K., and C. R. Stanley, 2007, Lithogeochemistry and hydrothermal alteration at the Halfmile Lake south deep zone, a volcanic-hosted massive sulfide deposit, Bathurst Mining Camp, New Brunswick: Exploration and Mining Geology, **15**, 177–199.
Moser, T. J., and C. B. Howard, 2008, Diffraction imaging in depth: Geophysical Prospecting, **56**, 627–641.
Pretorius, C. C., A. Jamison, and C. Irons, 1989, Seismic exploration in the Witwatersrand basin, Republic of South Africa: Proceedings of Exploration 87, Ontario Geological Survey, Special Volume 3, 241–253.
Pretorius, C. C., M. R. Muller, M. Larroque, and C. Wilkins, 2003, A review of 16 years of hardrock seismics on the Kaapvaal Craton, *in* D. W. Eaton, B. Milkereit, and M. H. Salisbury, eds., Hardrock seismic exploration: SEG, 247–268.
Roberts, B., E. Zaleski, G. Perron, E. Adam, L. Petrie, and M. Salisbury, 2003, Seismic exploration of the Manitouwadge Greenstone Belt, Ontario: A case history, *in* D. W. Eaton, B. Milkereit, and M. H. Salisbury, eds., Hardrock seismic exploration: SEG, 110–126.
Salisbury, M. H., C. W. Harvey, and L. Matthews, 2003, The acoustic properties of ores and host rocks in hardrock terranes, *in* D. W. Eaton, B. Milkereit, and M. H. Salisbury, eds., Hardrock seismic exploration: SEG, 9–19.
Salisbury, M. H., B. Milkereit, G. Ascough, R. Adair, L. Matthews, D. R. Schmitt, J. Mwenifumbo, D. W. Eaton, and J. Wu, 2000, Physical properties and seismic imaging of massive sulfides: Geophysics, **65**, 1882–1889.
Salisbury, M. H., and D. Snyder, 2007, Application of seismic methods to mineral exploration, *in* W. D. Goodfellow, ed., Mineral deposits of Canada: A synthesis of major deposit types, district metallogeny, the evolution of geological provinces, and exploration methods: Geological Association of Canada, Mineral Deposits Division, Special Publication 5, 971–982.
Schmelzbach, C., H. Horstmeyer, and C. Juhlin, 2007, Shallow 3D seismic-reflection imaging of fracture zones in crystalline rock: Geophysics, **72**, no. 6, B149–B160.
Sheriff, R. E., and L. P. Geldart, 1995, Exploration seismology: Cambridge University Press.
Stevenson, F., R. M. A. Higgs, and R. J. Durrheim, 2003, Seismic imaging of precious and base-metal deposits in Southern Africa, *in* D. W. Eaton, B. Milkereit, and M. H. Salisbury, eds., Hardrock seismic exploration: SEG, 141–156.
Stolt, R. H., 1978, Migration by Fourier transform: Geophysics, **43**, 23–48.
Stolt, R. H., and A. K. Benson, 1986, Seismic migration: Theory and practice: Geophysical Press.
Thomas, M. D., J. A. Walker, P. Keating, R. Shives, F. Kiss, and W. D. Goodfellow, 2000, Geophysical atlas of massive sulphide signatures, Bathurst Mining Camp, New Brunswick: Geological Survey of Canada Open File Report 3887.
Tryggvason, A., A. Malehmir, J. Rodriguez-Tablante, C. Juhlin, and P. Weihed, 2006, Reflection seismic investigation in the western part of the Paleoproterozoic VHMS-bearing Skellefte district, northern Sweden: Economic Geology, **101**, 1039–1054.
Verpaelst, P., A. S. Peloquin, E. Adam, A. E. Barnes, J. N. Ludden, D. J. Dion, C. Hubert, B. Milkereit, and M. Labrie, 1995, Seismic reflection profiles across the "Mine Series" in the Noranda camp of the Abitibi belt, eastern Canada: Canadian Journal of Earth Sciences, **32**, 167–176.
Widess, M. B., 1973, How thin is a thin bed?: Geophysics, **38**, 1176–1180.
Wu, J., B. Milkereit, and D. E. Boerner, 1995, Seismic imaging of the enigmatic Sudbury structure: Journal of Geophysical Research, **100**, 4117–4130.
Yilmaz, O., 2001, Seismic data analysis: Processing, inversion, and interpretation of seismic data: SEG.